J|A|C|S
ARTICLES
Published on Web 12/02/2004

Preparation and Characterization of the Native Iron(II)-Containing DNA Repair AlkB Protein Directly from *Escherichia coli*

Yukiko Mishina,[§] Lin X. Chen,*[,†] and Chuan He*[,§]

Contribution from the Department of Chemistry, The University of Chicago, Chicago, Illinois 60637, and Chemistry Division, Argonne National Laboratory, Building 200, 9700 South Cass Avenue, Argonne, Illinois 60439

Received August 16, 2004; E-mail: chuanhe@uchicago.edu (C.H.); lchen@anl.gov (L.X.C.)

Abstract: The *Escherichia coli* AlkB protein was recently found to repair cytotoxic DNA lesions 1-methyladenine and 3-methylcytosine by using a novel iron-catalyzed oxidative demethylation mechanism. This protein belongs to a family of 2-ketoglutarate−Fe(II)-dependent dioxygenase proteins that utilize iron and 2-ketoglutarate to activate dioxygen for oxidation reactions. We report here the overexpression and isolation of the native Fe(II)−AlkB with a bound cofactor, 2-ketoglutarate, directly from *E. coli*. UV−vis measurements showed an absorption peak at 560 nm, which is characteristic of a bidentate 2-ketoglutarate bound to an iron(II) ion. Addition of excess amounts of single-stranded DNA to this isolated Fe(II)−AlkB protein caused a 9 nm shift of the 560 nm band to a higher energy, indicating a DNA-binding-induced geometry change of the active site. X-ray absorption spectra of the active site iron(II) in AlkB suggest a five-coordinate iron(II) center in the protein itself and a centrosymmetric six-coordinate iron(II) site upon addition of single-stranded DNA. This geometry change may play important roles in the DNA damage-searching and damage-repair functions of AlkB. These results provide direct evidence for DNA binding to AlkB which modulates the active site iron(II) geometry. The isolation of the native Fe(II)−AlkB also allows for further investigation of the iron(II) center and detailed mechanistic studies of the dioxygen-activation and damage-repair reactions performed by AlkB.

1. Introduction

Cellular DNA can be alkylated by intracellular and extracellular alkylation agents. Much of the alkylated damage, if not repaired, will have cytotoxic or mutagenic consequences. Cells have evolved dedicated systems to repair DNA alkylation damage.[1,2] In *E. coli*, an adaptive response pathway exists to protect DNA against high levels of alkylation damage.[3] Upon treatment with methylating reagents, the expression of four proteins, Ada, AlkA, AlkB, and AidB, are upregulated in *E. coli* through an Ada-regulated transcriptional activation pathway. Ada also repairs methylphosphotriester, O^6-methylguanine, and O^4-methylthymine lesions in DNA. AlkA is a glycosylase that excises N^3-methyladenine and related lesions from DNA in the first step of base excision repair. The function of AidB is still unknown. The function of the AlkB protein has been a mystery for a long time. The involvement of *E. coli* AlkB in DNA repair was proposed nearly two decades ago.[3] Earlier work from several groups demonstrated that this protein probably repairs single-stranded (ss) DNA damage, which tends to be induced by S_N2-type methylating agents.[4−8]

A recent computational protein-folding analysis of AlkB helped to partially unveil the function of this protein. AlkB was shown to have a sequence homologous to the 2-ketoglutarate−Fe(II)-dependent dioxygenase superfamily.[9] Subsequently in 2002, two groups discovered the function of AlkB through biochemical studies.[10,11] They found that AlkB repairs N^1-methyladenine and N^3-methylcytosine lesions in DNA (Figure 1). The protein utilizes iron, dioxygen, and 2-ketoglutarate and was proposed to perform an unprecedented oxidative dealkylation repair of the base lesions (Figure 1). With 2-ketoglutarate providing two extra electrons, a putative iron(IV) oxene intermediate was thought to form from the reaction of an active site iron(II) with dioxygen. The high-valent iron−oxo species generated from the dioxygen-activation reaction could then hydroxylate the methyl group on the nitrogen of the base. Subsequent decomposition of the resulting product gives formaldehyde and a dealkylated base. It was demonstrated that

[§] The University of Chicago.
[†] Argonne National Laboratory.

(1) Friedberg, E. C.; Walker, G. C.; Siede, W. *DNA Repair and Mutagenesis*; ASM Press: Washington, DC, 1995.
(2) Wood, R. D.; Mitchell, M.; Sgouros, J.; Lindahl, T. *Science* **2001**, *291*, 1284−1289.
(3) Lindahl, T.; Sedgewick, B.; Sekiguchi, M.; Nakabeppu, Y. *Annu. Rev. Biochem.* **1988**, *57*, 133−157.
(4) Kondo, H.; Nakabeppu, Y.; Kataoka, H.; Kuhara, S.; Kawabata, S.; Sekiguchi, M. *J. Biol. Chem.* **1986**, *261*, 15772−15777.
(5) Dinglay, S.; Trewick, S. C.; Lindahl, T.; Sedgwick, B. *Genes Dev.* **2000**, *14*, 2097−2105.
(6) Samson, L.; Derfler, B.; Waldstein, E. A. *Proc. Natl. Acad. Sci. U.S.A.* **1986**, *83*, 5607−5610.
(7) Wei, Y.-F.; Carter, K. C.; Wang, R.-P.; Shell, B. K. *Nucleic Acids Res.* **1996**, *24*, 931−937.
(8) Dinglay, S.; Gold, B.; Sedgwick, B. *Mutat. Res.* **1998**, *407*, 109−116.
(9) Aravind, L.; Koonin, E. V. *GenomeBiology* **2001**, *2*, 007.001−007.008.
(10) Trewick, S. C.; Henshaw, T. F.; Hausinger, R. P.; Lindahl, T.; Sedgwick, B. *Nature* **2002**, *419*, 174−178.
(11) Falnes, P. O.; Johansen, R. F.; Seeberg, E. *Nature* **2002**, *419*, 178−182.

10.1021/ja045066z CCC: $27.50

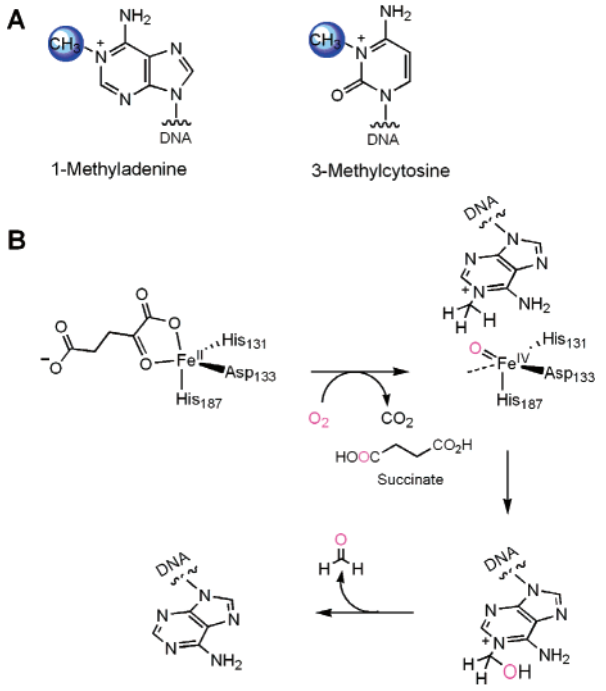

Figure 1. (A) DNA base lesions repaired by AlkB. (B) The proposed active site structure and repair mechanism of AlkB.

ssDNA, double-stranded DNA, and even RNA base lesions could be repaired by AlkB.[10−12] This protein also catalyzes the dealkylation of N^1-methyl-dAMP(5′) and N^1-methyl-dATP.[13] AlkB appears to be widely conserved in different organisms. Three homologues have also been found in humans.[7,12,14] Among them, the functions of two have been determined to be similar to that of *E. coli* AlkB.[12,14]

Previously, we performed a chemical cross-linking study on AlkB and confirmed that the three conserved residues, His131, Asp133, and His187, are active site residues.[15] The study also provided insight into the substrate preferences and the damage-searching mechanism of this protein; AlkB seems to work on ssDNA and dsDNA with a damaged base on an unstable base pair. Cross-linking studies on the human AlkB homologues revealed similar properties.[16] Despite recent activity studies on AlkB, the iron-containing active site in AlkB has yet to be characterized with spectroscopic methods. The proposed repair mechanism of AlkB and its interaction with DNA have not been subjected to detailed spectroscopic and mechanistic evaluations. Meanwhile, the structure of the iron(II) active site in AlkB has yet to be characterized. In fact, iron-containing AlkB has not been isolated before this report. Previous purification methods utilized recombinant AlkB constructs that bear an N-terminal His_6-tag. The overexpressed proteins were purified by metal-affinity columns, which may disrupt the binding of iron(II) to AlkB. All of the reported activity studies on AlkB were performed with the addition of free iron(II), 2-ketoglutarate, a reducing agent and substrate to apo-AlkB.[10,11,13,17] If the wild-type AlkB protein with bound iron(II) and 2-ketoglutarate cofactor can be prepared and purified directly from *E. coli*, the active iron(II) center could be characterized with various spectroscopic methods. This would also provide, in a straightforward manner, a native AlkB protein containing 2-ketoglutarate-bound iron(II) for careful evaluation of the protein reaction mechanism.

Here we report the preparation and isolation of the wild-type AlkB from *E. coli* with a bound iron(II) and cofactor. An absorption peak at 560 nm in the UV−vis spectrum of this protein was observed, which is a characteristic of the charge transfer from iron(II) to a bound 2-ketoglutarate. Addition of ssDNA shifted the absorption maximum slightly to a higher energy. The local structure of the iron(II) center was characterized with iron K-edge X-ray absorption spectroscopy in the absence and presence of ssDNA. In the absence of DNA, the AlkB active site can be best described as a five-coordinate iron(II) center. Binding of the DNA induces a geometry change in the active site where the iron(II) center adopts a more centrosymmetric octahedral coordination geometry.

2. Experimental Section

2.1. Construction, Expression, and Purification of AlkB Proteins. The *E. coli* AlkB gene was cloned into the *Hin*dIII and *Nde*I sites of a pET30a vector (Novagen). *E. coli* BL21(DE3) were transformed with the vector, and positive clones were selected from LB-agar plates containing kanamycin (50 μM). The cells were grown at 37 °C in the presence of kanamycin (50 μM) until the OD_{600} was 0.6. IPTG (1 mM) and $FeSO_4$ (5 μM) were added, and the cells were grown for an additional 4 h at 30 °C. All subsequent steps were performed at 4 °C in the presence of 10 mM 2-mercaptoethanol. The cells were harvested by centrifugation and stored at −80 °C. The cell pellet was resuspended in 30 mL of lysis buffer (10 mM Tris [pH 7.34], 300 mM NaCl, 5% glycerol, 2 mM $CaCl_2$, 10 mM $MgCl_2$, 10 mM 2-mercaptoethanol), disintegrated by sonication, and centrifuged at 12 000 rpm for 20 min. The supernatant was centrifuged at 3000 rpm for another 20 min with the addition of DEAE−cellulose. The supernatant was then added to 3 vol of buffer A (10 mM Tris−HCl [pH 7.34]), loaded onto an SP Sepharose cation exchange column (Amersham Pharmacia, 25 mL) that had been equilibrated with buffer A, and eluted with a linear gradient of NaCl (0.0−1.0 M in 180 mL). The fractions (10 mL per fraction) containing the protein were diluted by buffer A and purified immediately with the Mono-S cation exchange column (Amersham Pharmacia, 1 mL) using a linear gradient of NaCl (0.0−1.0 M in 20 mL). The resulting pink fractions (1 mL per fraction) were collected and concentrated for spectroscopic studies. About 3 mg of pure protein could be obtained from 1 L of wet cells by following this purification procedure. Point mutations in AlkB (H131C, D133C, and H187C) were introduced by megaprimer mutagenesis. The sequences of the wild-type and mutant AlkB were confirmed by sequencing the entire coding sequence. The mutant proteins were purified following the same procedure as that of the wild-type protein. They all showed indistinguishable chromatographic behavior from that of wild-type AlkB.

2.2. Iron Content Quantification, UV−vis, and Isothermal Titration Calorimetry (ITC) Studies. The AlkB concentration was determined by amino acid analysis (Texas A&M University, Protein Technologies Facility Core). The calculated extinction coefficient (ϵ_{280}) and the BCA assay (Pierce) were calibrated using this result and have been subsequently employed to measure the concentration of the protein. The equivalents of the bound iron for the wild-type AlkB protein and

(12) Aas, P. A.; Otterlei, M.; Falnes, P. O.; Vagbo, C. B.; Skorpen, F.; Akbari, M.; Sundheim, O.; Bjoras, M.; Slupphaug, G.; Seeberg, E.; Krokan, H. E. *Nature* **2003**, *421*, 859−863.
(13) Koivisto, P.; Duncan, T.; Lindahl, T.; Sedgwick, B. *J. Biol. Chem.* **2003**, *278*, 44348−44354.
(14) Duncan, T.; Trewick, S. C.; Koivisto, P.; Bates, P. A.; Lindahl, T.; Sedgwick, B. *Proc. Natl. Acad. Sci. U.S.A.* **2002**, *99*, 16660−16665.
(15) Mishina, Y.; He, C. *J. Am. Chem. Soc.* **2003**, *125*, 8730−8731.
(16) Mishina, Y.; Lee, C.-H. J.; He, C. *Nucleic Acids Res.* **2004**, *32*, 1548−1554.
(17) Welford, R. W. D.; Schlemminger, I.; McNeill, L. A.; Hewitson, K. S.; Schofield, C. J. *J. Biol. Chem.* **2003**, *278*, 10157−10161.

each of the mutant proteins were quantified by ICP−MS at STAT-ANALYSIS Corporation. The UV−vis spectrum of Fe(II)−AlkB was recorded after the protein was purified and concentrated to 1.0 mM in a standard storage buffer (10 mM Tris [pH 7.34], 300 mM NaCl, 10 mM 2-mercaptoethanol) at 4 °C. The UV−vis spectrum of Fe(II)−AlkB with ssDNA was recorded under the same conditions in the presence of 1.0 mM AlkB and 4.1 mM ssDNA 5′-TTTTTCTTTTT.

Isothermal titration calorimetry experiments were performed on a MicroCal VP−ITC microcalorimeter at 6 °C and analyzed using the MicroCal Origin software. The DNA (TTTTTCTTTTT) was dissolved into the same buffer as the AlkB for each experiment (10 mM Tris [pH 7.34], 100 mM NaCl for experiments with apo-AlkB, and 10 mM Tris [pH 7.34], 100 mM NaCl, 10 mM 2-mercaptoethanol for experiments involving Fe(II)). Each experiment was performed in duplicate. Each titration consisted of 10 μL injections of 1 mM DNA into a 1.4 mL sample cell consisting of 0.12−0.16 mM AlkB sample. The association constant (K_a) was obtained directly from the data, and the dissociation constant (K_d) was calculated as $1/K_a$.

2.3. X-ray Absorption Spectroscopy. Iron K-edge X-ray absorption near edge structure (XANES) and X-ray absorption fine structure (XAFS) spectra were collected at the Beamline 12BM of the Advanced Photon Source, Argonne National Laboratory. Si(111) crystals were used in the monochromator. A Pt-coated mirror was used to focus the beam and to remove higher harmonic X-ray photons. The beam size at the sample was approximately 0.4 mm(v) × 1 mm(h). A feedback system was used to control the monochromator crystal angle and was set to 70% detuning. A 13-element germanium solid-state detector (Canberra) was used to collect iron X-ray fluorescence signals. A manganese filter was placed in front of the detector with Soller slits for attenuation of elastic scatterings, which increased the signal ratio between the fluorescence and the elastic scattering of the sample from <1:100 to ~1:1. The outputs from the amplifiers of the detector were connected to an array of single channel analyzers (SCA) with upper and lower thresholds set to allow only $K_{\alpha 1}$ and $K_{\alpha 2}$ fluorescence signals to be further processed. An ion chamber was placed before the sample for the incident X-ray flux reference signal, I_0, and the second and the third ion chambers were placed after the sample. An iron foil inserted between the second and the third ion chambers was used for the energy calibration. The output signals from the SCAs were connected to a scalar array that interfaced with a computer hosting a data acquisition program (G. Jennings, Argonne National Laboratory).

The freshly purified Fe(II)−AlkB (1.2 mM in 10 mM Tris [pH 7.34], 300 mM NaCl, 20% glycerol, and 10 mM 2-mercaptoethanol) and Fe(II)−AlkB/DNA (0.9 mM/3.4 mM, DNA = 5′-TTTTTCTTTTT) samples were enclosed respectively by sample cells with Mylar windows. The sample cell was mounted on a copper sample holder attached to a close-cycle cryogenic system (Janis).

Conventional XAFS data analysis programs, WinXAS (T. Ressler), and FEFF8 (University of Washington) were used in data analysis for the protein samples and XAFS spectra simulation of the reference compound. Because neither the crystal structure nor the tertiary structure around iron(II) is known, a reference structure of the iron(II) site[18] was constructed using the Material Studio modeling program (Accelry) by positioning the most likely ligands, two His residues, one Asp residue, and one 2-ketoglutarate around iron(II) (Figure S1 of the Supporting Information). Two N_ϵ atoms of the two His residues, one O_δ atom of the Asp, and two O atoms of 2-ketoglutarate are directly ligated with iron(II) in the reference structure. The FEFF8 program was used to generate X-ray scattering paths for the references of the fitting. Three single scattering paths from the nearest Fe−N and Fe−O and the next nearest Fe−C, as well as one multiple scattering path of Fe−N(O)−C, are used to fit the first two peaks in the FT−XAFS spectra (R = 1.0−2.5 Å, without phase correction). The calculated parameters for two scattering paths (Fe−O and Fe−N) were chosen for modeling the nearest neighbors, and parameters for one Fe−C single scattering path and one Fe−N(O)−C multiple scattering path were used for modeling the next nearest neighbors. Subsequent fittings with WinXAS (T. Ressler) to the raw spectra were carried out. The same paths are used for the protein with and without DNA. An attempt was made to fit the entire unfiltered spectra, which require at least four single scattering paths and two multiple scattering paths (Figure S2 and Table S1 of the Supporting Information), but the data quality at higher k as well as the diversity of the ligand structures prevented reliable structural parameters for distant atoms to be extracted despite the apparent fits. Therefore, we chose to present the results from fitting the first two peaks of the FT−XAFS spectra.

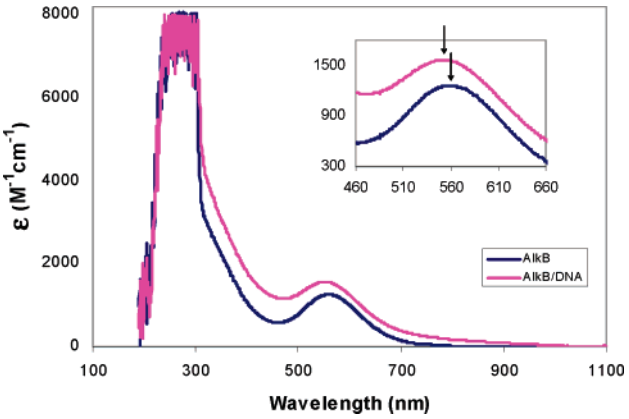

Figure 2. The UV−vis spectra of Fe(II)−AlkB (1.0 mM) in the absence and presence of ssDNA (4.1 mM) recorded at 4 °C. Inset: magnified view of the plots from 460 to 660 nm.

3. Results and Discussion

3.1. Isolation of the Iron(II)-Containing AlkB, Its UV−vis Spectrum, and Its Binding to Single-Stranded DNA. The wild-type AlkB (Met1-Glu216) was overexpressed in the presence of 5 μM $FeSO_4$ from *E. coli* with no tag. The protein could be purified to >90% purity using two rounds of cation exchange column purification (Figure S3 of the Supporting Information). Pink/purple fractions of the purified protein were easily visible if the whole purification procedure was done within 5 h in the presence of 10 mM 2-mercaptoethanol at 4 °C. The iron content of the isolated AlkB was quantified by ICP−MS to be approximately 0.54 equiv per protein (an average of three samples). The absorption spectrum of this isolated iron-(II)-containing AlkB showed a peak at 560 nm with ϵ = 1258 M^{-1} cm^{-1} (Figure 2; the extinction coefficient was calculated based on the iron(II) content). This peak was assigned as the iron(II) to 2-ketoglutarate charge-transfer based on the observation and assignment of similar peaks for other 2-ketoglutarate−Fe(II)-dependent dioxygenase proteins and model compounds. It is known that this peak is diagnostic of a 2-keto acid chelate to an iron(II) center.[19−24] Addition of 2 mM EDTA completely abolished the color of the Fe(II)−AlkB solution. On the basis of these observations and previous knowledge, we believe a

(18) Henshaw, T. F.; Feig, M.; Hausinger, R. P. *J. Inorg. Biochem.* **2004**, *98*, 856−861.

(19) Ryle, M. J.; Padmakumar, R.; Hausinger, R. P. *Biochemistry* **1999**, *38*, 15278−15286.
(20) Hikichi, S.; Ogihara, T.; Fujisawa, K.; Kitajima, N.; Akita, M.; Moro-oka, Y. *Inorg. Chem.* **1997**, *36*, 4539−4547.
(21) Hegg, E. L.; Ho, R. Y. N.; Que, L. J. *J. Am. Chem. Soc.* **1999**, *121*, 1.
(22) Ha, E. H.; Ho, R. Y. N.; Kisiel, J. F.; Valentine, J. S. *Inorg. Chem.* **1995**, *34*, 2265−2266.
(23) Chiou, Y.-M.; Que, L. J. *J. Am. Chem. Soc.* **1995**, *117*, 3999−4013.
(24) Chiou, Y.-M.; Que, L. J. *J. Am. Chem. Soc.* **1992**, *114*, 7567−7568.

2-ketoglutarate-bound iron(II) site was retained in the AlkB protein purified directly from *E. coli*.

A similar peak with the maximum absorption at 500 nm was reported previously for an apo-AlkB incubated with free iron(II) and excess amounts of 2-ketoglutarate.[10] This peak was recorded as a difference spectrum of anaerobic AlkB (0.35 mM) in the presence of 2-ketoglutarate (1 mM) and iron(II) (0.3 mM) minus the spectrum without iron(II). The absorption maximum of this previously reported peak was shifted (60 nm) compared to the spectrum recorded here with the Fe(II)−AlkB isolated directly from *E. coli*. In the previous study, iron(II) and the excess amounts of 2-ketoglutarate were added externally to apo-AlkB. In our protein sample, there is no externally added iron(II). Instead, Fe(II)−AlkB was isolated and purified directly from *E. coli* cells. We think the spectrum of this iron(II)-containing AlkB represents the native state of the iron(II) to the 2-ketoglutarate charge-transfer band. This offers an opportunity to perform spectroscopic and mechanistic studies on AlkB with well-defined bound iron(II) and the cofactor 2-ketoglutarate.

The iron(II)-bound AlkB was reasonably stable at 4 °C in the presence of 10 mM 2-mercaptoethanol at concentrations up to 2 mM. At 4 °C, the absorption peak intensity at 560 nm did not change considerably after 3 h. At room temperature, the protein tends to aggregate and precipitate at high concentrations. Recently, it was shown that AlkB can catalyze an aberrant oxidation of Trp178 to give a blue chromophore (λ_{max} 580 nm, $\epsilon \sim 1000\ M^{-1}\ cm^{-1}$) upon reacting with oxygen-saturated water.[18] The color comes from a ligand-to-metal charge-transfer band involving OH−Trp binding to an iron(III) center.[25] The Fe(II)−AlkB samples studied here have always been kept under reducing conditions. It is very clear from the X-ray absorption studies that the active site iron is at the iron(II) oxidation state. We did not observe the aberrant oxidation under our experimental conditions.

The UV−vis spectrum of Fe(II)−AlkB in the presence of ssDNA was recorded. The charge transfer band at 560 nm was shifted to 551 nm immediately after the addition of an excess amount of ssDNA (Figure 2). The peak was also broadened in the presence of ssDNA. Excess amounts of DNA were used to ensure the binding of AlkB with DNA. The observed spectrum change upon addition of DNA suggested that DNA binding to AlkB might have induced a geometry change in the iron(II) center in AlkB that affected the interaction between the iron(II) and its cofactor. This potential geometry change was investigated by X-ray absorption spectroscopy, as described in the next section.

Three mutant AlkB proteins, H131C, D133C, and H187C, with the three putative active site ligands, His131, Asp133, and His187, mutated to Cys residues, respectively, were also overexpressed and purified. No color was observed for these mutant proteins. No iron was found in these mutants from ICP−MS measurements. The mutation of the active site ligands to Cys residues might have disrupted the binding of iron(II). This result is consistent with the assignment of the three residues as the active site ligands.

The binding of the apo-AlkB to an 11-mer ssDNA was measured by ITC experiments at 6 °C. A K_d of 30 ± 7 μM was obtained in duplicate studies (Figure S4 of the Supporting Information). We also performed ITC experiments on the purified Fe(II)−AlkB protein (with 0.54 equiv of bound iron(II)) and the same ssDNA. A very similar association constant was obtained (43 ± 14 μM, Figure S4). The result indicates that the protein will bind ssDNA under conditions in which our X-ray absorption studies would be performed.

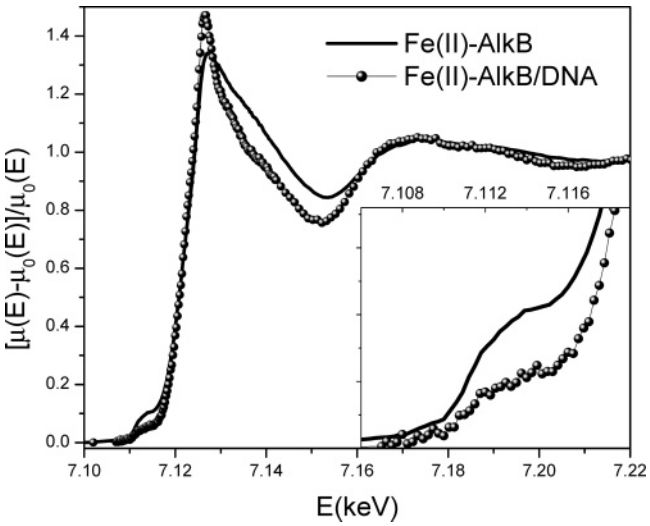

Figure 3. XANES spectra of Fe(II)−AlkB with and without the ssDNA. The inset shows the pre-edge feature that is attenuated due to the DNA binding. The higher oscillation amplitude with the DNA binding hints an increase in the coordination number, presumably from the nearest neighbors.

3.2. XANES Features. X-ray absorption spectra of Fe(II)−AlkB (1.2 mM) and Fe(II)−AlkB with 3.8 equiv of ssDNA TTTTTCTTTTT were measured respectively at 15 K within 2−3 h after each protein was purified (Figure 3); minimum change of the UV−vis absorption was observed for these samples compared to the same sample right after the purification. The transition edge positions in both spectra confirm the iron(II) oxidation states in both samples in comparison with literature[26,27] and with the iron(II) sites in bacterial photosynthetic reaction center proteins.[28] The pre-edge features from 7.180 to 7.20 keV arise from the 1s → 3d transitions through quardrupole interactions. Because this transition is formally electric dipole forbidden, typical pre-edge features of a centrosymmetric octahedral iron(II) complex are very weak. In comparison, the pre-edge features for noncentrosymmetric iron(II) complexes, such as a square pyramidal or a tetrahedral coordination, show enhanced pre-edge intensities due to the mixing of the 4p orbitals into the 3d orbitals, which introduces the dipole allowed 1s → 4p transition component with much higher intensity.[26,27]

The pre-edge peak intensity of Fe(II)−AlkB between 7.18 and 7.20 keV is much more pronounced than that of the Fe(II)−AlkB with 3.8 equiv of ssDNA, indicating a more centrosymmetric coordination geometry around the iron(II) atom in the latter. These observations suggest that a less symmetric iron(II) center with four or five ligands in Fe(II)−AlkB likely becomes a more centrosymmetric octahedral site when binding to ssDNA. The white light peak of the DNA-containing sample sharpens

(25) Liu, A.; Ho, R. Y. N.; Que, L., Jr.; Ryle, B. S.; Phinney, R. P.; Hausinger, R. P. *J. Am. Chem. Soc.* **2001**, *123*, 5126−5127.

(26) Kemsley, J. N.; Zaleski, K. L.; Chow, M. S.; Decker, A.; Shishova, E. Y.; Wasinger, E. C.; Hedman, B.; Hodgson, K. O.; Solomon, E. I. *J. Am. Chem. Soc.* **2003**, *125*, 10810−10821.

(27) Westre, T. E.; Kennepohl, P.; DeWitt, J. G.; Hedman, B.; Hodgson, K. O.; Solomon, E. I. *J. Am. Chem. Soc.* **1997**, *119*, 6297−6314.

(28) Chen, L. X.; Utschig, L. M.; Schelesselman, S. L.; Tiede, D. M. *J. Phys. Chem. B* **2004**, *108*, 3912−3924.

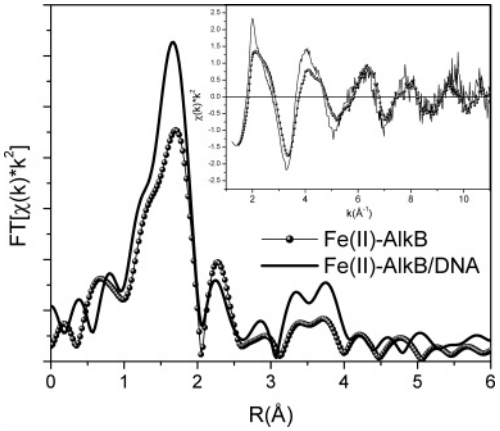

Figure 4. FT−XAFS spectra of Fe(II)−AlkB and Fe(II)−AlkB/DNA without phase correction. A clear correspondence between two sets of peaks can be seen, with an increase of the nearest neighbor peak (1.7 Å) upon DNA binding. The next nearest neighbor peak decreases slightly, suggesting disturbance of the ligands due to the DNA binding. The identity of a distant peak between 3 and 4 Å is unclear due to the unknown information of protein tertiary structure. Inset: XAFS spectra of Fe(II)−AlkB and Fe(II)−AlkB/DNA with k^2 weighting. The oscillation amplitude increases upon the DNA binding, indicating an increase of the coordination number of the iron(II) center.

considerably compared to that for the protein alone (Figure 3), which is consistent with an increase of the coordination number of the iron(II) site upon binding with DNA.

3.3. XAFS Spectra. XAFS spectra of Fe(II)−AlkB and Fe(II)−AlkB/DNA with k^2 weighting are depicted in Figure 4. The oscillation amplitude increases upon DNA binding, suggesting an increase in the coordination number of the iron(II) center. The enhanced amplitude for the peak around $R = 1.7$ Å (without phase correction) in the Fourier transformed XAFS spectra (Figure 4) for the Fe(II)−AlkB/DNA complex relative to that of Fe(II)−AlkB clearly corresponds to an increase in the coordination number for the nearest neighbors of iron(II). The second peak reduces upon DNA binding, which is likely due to an increase of the Debye−Waller factor from the enhanced structural heterogeneity of the second shell neighbors upon the binding. The identity of the third peak between $R = 3-4$ Å is unclear without the crystal structure of this protein. Obviously, this third peak is also enhanced in amplitude due to the DNA binding. The shapes and the positions of the second and third peaks in Figure 4 are similar between two separate measurements conducted on different dates, and their intensities differ beyond the noise level of the data. These similarities and differences validate the reliability of the data.

The structural parameters of the iron(II) site in each sample are extracted by fitting the function mentioned in the Experimental Section to the back Fourier transformed spectra in Figure 4, with a window of $R = 1.0-2.5$ Å. The structural parameters extracted from the results of the fits are listed in Table 1, and the agreement between the experimental data and the fitting curves is shown in Figure 5. To fit the spectra in Figure 5, three single scattering paths and one multiple scattering path are used. The structural parameters from the phenomenological fits should be viewed with caution due to the lack of a tertiary structure of this protein. The nearest neighbor distances (Fe−N and Fe−O) for Fe(II)−AlkB fit a two-distance model with the coordination numbers of 2.2 and 2.6 and the distances of 1.94 and 2.13 Å, respectively. Upon binding with the DNA, only one of the nearest neighbor distances is affected preferentially with the

Table 1. Structural Parameters Extracted for Two Neighboring Shells around Fe(II)[a]

sample	coordination number	R (Å)	σ^2 (Å^2)[b]
Fe(II)−AlkB	2.4 ± 0.5	1.94 ± 0.02	0.006
	2.6 ± 0.5	2.13 ± 0.02	0.001
	1.6 ± 1.0	2.83 ± 0.04	0.00007
	9.1 ± 1.0 (MS)[c]	2.67 ± 0.04	0.002
Fe(II)−AlkB/DNA	3.4 ± 0.5	1.99 ± 0.02	0.01
	2.6 ± 0.6	2.12 ± 0.02	0.002
	2.1 ± 1.0	2.73 ± 0.04	0.008
	6.5 ± 1.0 (MS)[c]	2.67 ± 0.04	0.006

[a] Reference parameters are from four paths in FEFF-calculated iron(II) site structure simulated by positioning two His, one Asp, and one 2-ketoglutarateoxalate as the ligands. The simulated structure is included in the Supporting Information (Figure S1 and Table S1). The results of the fits are shown in Figure 5. [b] σ^2 is the Debye−Waller factor. [c] MS is multiple scattering.

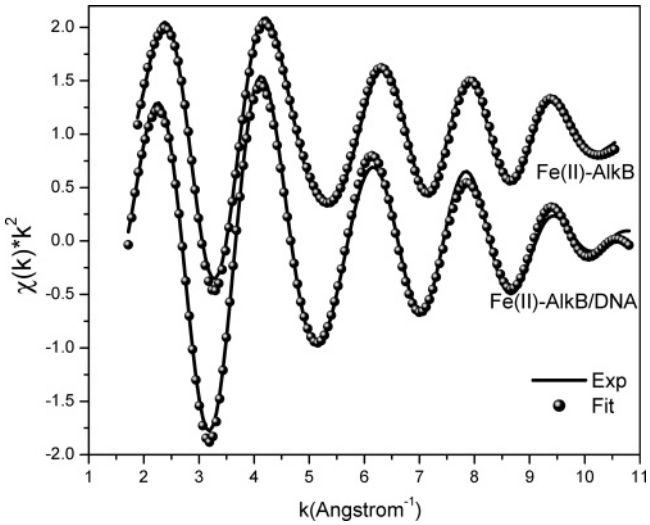

Figure 5. Isolated back FT−XAFS spectra for the nearest neighbors and next nearest neighbors ($R = 1.0-2.5$ Å in Figure 4) along with the fitting functions. The structural parameters are listed in Table 1.

coordination number and distance increased by 1 and 0.05 Å, respectively. These differences support an additional ligand binding with iron upon protein interaction with DNA. The structural parameters of the next nearest neighboring shell (Fe−C), although with less precision than the nearest neighbors because of the presumed asymmetry of the iron(II) site, show a 0.1 Å decrease in bond distance, while the multiple scattering (modeled by the Fe−N−C path) remains largely unchanged and reveals a decrease in coordination number upon the binding of the DNA. The coordination numbers for the second neighboring shell of about 2 are lower than those expected for available Fe−C distances, which may be due to the static Debye−Waller factor from the diversity of the distance. The apparent Fe−C distance of 2.83 Å agrees well with the Fe−C_δ (of His) distance in the reference (Figure S1), although the multiple path Fe−N−C distance is shorter than expected. Because the distances between the central iron(II) to other atoms could be much more heterogeneous than those presented in the model (Figure S1), and there are numerous ways to arrange the ligands to affect the appearance of XAFS spectra, this model should be viewed with caution, especially for those non-nearest neighboring atoms.

We have attempted to fit the spectra without the Fourier transform filter (Figure S2), but the choice of parameters is not unique for the distant atoms, and the confidence of the fitting is limited by the data quality in the high k region. Therefore, it

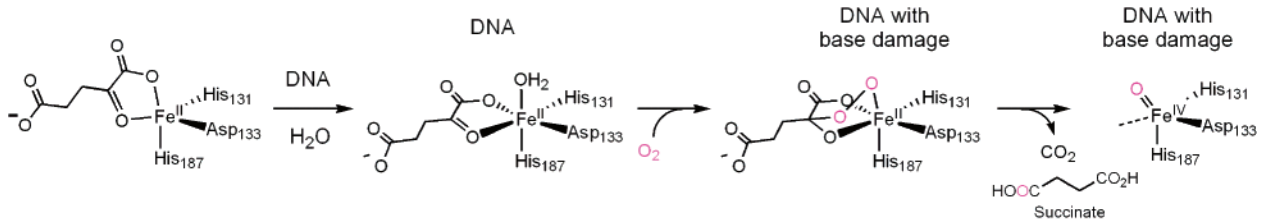

Figure 6. Proposed mechanism for DNA binding and dioxygen activation by AlkB.

is more accurate to focus on the first two peaks of the FT−XAFS spectra for the iron(II) with diverse ligand and unknown tertiary structure. Despite the uncertainty, the increase in the coordination number and the symmetry of the iron(II) site upon the DNA binding are evident from both the XANES and XAFS spectra. Apparently, the binding of DNA makes the iron(II) site of AlkB more central symmetric due to the addition of a ligand with concurrent increase on the coordination number and the bond distance for one of the two subgroups of the nearest neighbors.

3.4. DNA-Binding-Induced Conformation Change. The UV−vis study of Fe(II)−AlkB and Fe(II)−AlkB/DNA complexes suggests to us that a geometry change of the active site iron(II) may have taken place upon DNA binding. Such geometry change is further confirmed by the XANES and XAFS spectra of the iron(II) site in Fe(II)−AlkB and Fe(II)−AlkB/DNA complexes. The data indicate that the iron(II) center adopts a less symmetric five-coordinate site in the native Fe(II)−AlkB. The addition of ssDNA changed it to a more centrosymmetric six-coordinate iron(II) site (Figure 6). This provides direct spectroscopic evidence for DNA binding to AlkB. Also, it shows that DNA binding affects the geometry of the active site iron(II). These results further support the proposed function of AlkB. ITC experiments were performed to measure the dissociation constant of AlkB and the ssDNA used in the above studies. The result ($K_d \sim 30 \pm 7$ μM for apo-AlkB, 43 ± 14 μM for purified Fe(II)−AlkB) indicates binding of the ssDNA to AlkB in the UV−vis and X-ray absorption experiments.

The geometry change observed here is somewhat different from what has been proposed for other members of the 2-ketoglutarate−Fe(II)-dependent dioxygenase proteins that have been studied. Substrate binding of clavaminate synthase 2 (CS2) was investigated using circular dichroism (CD) and magnetic circular dichroism (MCD) techniques.[29,30] It was shown that the substrate binding to the iron(II)- and cofactor-bound protein induces a conversion of the iron(II) center from six- to five-coordinate. It was proposed that this geometry change creates a site on iron(II) for dioxygen binding. The observation of a six-coordinate iron(II) site with a bound cofactor, 2-ketoglutarate, in the crystal structure of a related protein, deacetoxycephalosporin C synthase (DAOCS), agrees with this mechanism.[31] Decrease of coordination number on the iron(II) center upon substrate binding was also proposed for (2,4-dichlorophenoxy)acetate/2-ketoglutarate dioxygenase (TfdA), taurine/2-ketoglutarate dioxygenase (TauD), and isopenicillin N synthase (IPNS).[19,32,33] However, it is interesting to note that the crystal structure of Fe(II)−TauD showed a five-coordinate iron(II) site with a bidentate-bound 2-ketoglutarate in the absence of substrate.[34]

What we have observed for AlkB indicates an increase in coordination number on the iron(II) site upon binding to ssDNA. The dioxygen activation for this group of dioxygenase proteins is likely to be regulated by the binding of substrate. Substrate binding may stimulate a conformational change that facilitates oxidation of the active site iron(II) by dioxygen. The six-coordinate iron(II) site, formed in AlkB upon binding of ssDNA, could be related to the unique function of AlkB. This protein works on macromolecule substrates; most other mononuclear iron-containing dioxygenases work on small molecules. A high turnover number may not be required for the damage-repair reaction catalyzed by AlkB since the damage-searching step is likely the rate-limiting step. It is known that AlkB does not catalyze the repair of a damaged base without the presence of a 5′ phosphate group.[13] Thus, binding to DNA could be the first signal that triggers AlkB to adopt a conformation for damage-searching. Once a damaged base is located, a second signal would initiate dioxygen activation chemistry. Furthermore, iron(II)−water bonds are known to be labile;[35] the ligand exchange from water to dioxygen may not be a limiting factor for the overall repair reaction if a six-coordinate iron(II) is used for dioxygen activation.

4. Conclusion

The oxidative dealkylation of damaged DNA bases exhibited by AlkB proteins represents a new type of DNA repair mode.[36−39] The biological importance of this novel repair function has been demonstrated and will continue to be explored. The discovery of this unique repair mode also expanded the functions performed by mononuclear iron-containing dioxygenase proteins. We have shown here that the wild-type *E. coli* AlkB protein with bound iron(II) and cofactor 2-ketoglutarate can be overexpressed and isolated from *E. coli*. This protein form provides great opportunities to study the metal center and perform mechanistic investigations of AlkB.

The purified protein exhibits an absorption peak that is typical for a charge-transfer band of a bidentate 2-ketoglutarate bound

(29) Solomon, E. I.; Brunold, T. C.; Davis, M. I.; Kemsley, J. N.; Lee, S.-K.; Lehnert, N.; Neese, F.; Skulan, A. J.; Yang, Y.-S.; Zhou, J. *Chem. Rev.* **2000**, *100*, 235−349.
(30) Zhou, J.; Gunsior, M.; Bachmann, B. O.; Townsend, C. A.; Solomon, E. I. *J. Am. Chem. Soc.* **1998**, *120*, 13539−13540.
(31) Valegard, K.; van Scheltinga, A. C. T.; Lloyd, M. D.; Hara, T.; Ramaswamy, S.; Perrakis, A.; Thompson, A.; Lee, H.-S.; Baldwin, J. E.; Schofield, C. J.; Hajdu, J.; Andersson, I. *Nature* **1998**, *394*, 805−809.
(32) Hegg, E. L.; Whiting, A. K.; Saari, R. E.; McCracken, J.; Hausinger, R. P.; Que, L. J. *Biochemistry* **1999**, *38*, 16714−16726.
(33) Roach, P. L.; Clifton, I. J.; Hensgens, C. M. H.; Shibata, N.; Schofield, C. J.; Hajdu, J.; Baldwin, J. E. *Nature* **1997**, *387*, 827−830.
(34) Elkins, J. M.; Ryle, M. J.; Clifton, I. J.; Dunning Hotopp, J. C.; Lloyd, J. S.; Burzaff, N. I.; Baldwin, J. E.; Hausinger, R. P.; Roach, P. L. *Biochemistry* **2002**, *41*, 5185−5192.
(35) Lippard, S. J.; Berg, J. M. *Principles of Bioinorganic Chemistry*; University Science Books: Mill Valley, CA, 1994.
(36) Begley, T. J.; Samson, L. D. *Nature* **2003**, *421*, 795−796.
(37) Margison, G. *DNA Repair* **2002**, *1*, 1057−1061.
(38) Begley, T. J.; Samson, L. D. *Trends Biochem. Sci.* **2003**, *28*, 2−5.
(39) Jiricny, J. *Curr. Biol.* **2002**, *12*, R846−R848.

to an iron(II) center. This peak, at 560 nm, may represent an accurate assignment for the native Fe(II)−AlkB. The addition of ssDNA to Fe(II)−AlkB slightly shifted the charge-transfer band of AlkB, indicating a DNA-binding-mediated active site geometry change. This change was investigated by X-ray absorption spectroscopy. The native Fe(II)−AlkB was shown to contain a five-coordinate iron(II) center bound by oxygen and nitrogen ligands. Addition of ssDNA induced a different geometry of the active site iron(II), as revealed from X-ray absorption studies. A more centrosymmetric six-coordinate iron(II) center formed upon DNA binding. These results provide spectroscopic evidence for a DNA-binding-induced conformation change of AlkB. This change may have a significant implication for the function of AlkB. It is possible that AlkB adopts a six-coordinate iron(II) site while searching for damaged bases in DNA.

Acknowledgment. This work was supported by the University of Chicago (C.H.) and by the Division of Chemical Sciences, Office of Basic Energy Sciences, the U.S. Department of Energy under contract W-31-109-ENG-38 (L.X.C.). C.H. is a 2003 Searle Scholar, a 2004 G&P Foundation for Cancer Research Young Investigator, and a 2004 W. M. Keck Foundation Distinguished Young Scholar in Biomedical Research. Use of the Advanced Photon Source was supported by the U.S. Department of Energy, Office of Science, Office of Basic Energy Sciences, under Contract W-31-109-ENG-38. We thank Dr. Jennifer Linton and other BESSRC-CAT beamline personnel for their support during the experiments. We also thank Dr. M. A. Yousef for help in ITC experiments performed at the Biophysical Core Facility at the University of Chicago.

Supporting Information Available: Figures S1−S4 and Table S1. This material is available free of charge via Internet at http://pubs.acs.org.

JA045066Z